This article has been accepted for publication in a future issue of this journal, but has not been fully edited. Content may change prior to final publication. Citation information: DOI 10.1109/TBME.2015.2465855, IEEE Transactions on Biomedical Engineering

Fast Rotation-Free Feature Based Image Registration Using Improved N-SIFT and GMM Based Parallel Optimization

Dongdong Yu[1], Feng Yang[1,*], Caiyun Yang, Chengcai Leng, Jian Cao, Yining Wang, and Jie Tian*, *IEEE Fellow*

***Abstract*—Image registration is a key problem in a variety of applications, such as computer vision, medical image processing, pattern recognition, etc., while the application of registration is limited by time-consumption and the accuracy in the case of large pose differences. Aimed at these two kinds of problems, we propose a fast rotation-free feature based rigid registration method based on our proposed accelerated-NSIFT (A-NSIFT) and GMM Registration based Parallel Optimization (PO-GMMREG). Our method is accelerated by using the GPU/CUDA programming and preserving only the location information without constructing the descriptor of each interest point, while its robustness to missing correspondences and outliers is improved by converting the interest point matching to Gaussian mixture model alignment. The accuracy in the case of large pose differences is settled by our proposed PO-GMMREG algorithm by constructing a set of initial transformations. Experimental results demonstrate that our proposed algorithm can fast rigidly register 3D medical images and is reliable for aligning 3D scans even when they exhibit a poor initialization.**

Manuscript received December 2, 2014; revised April 8, 2015 and June 13, 2015; accepted July 29, 2015. This paper is supported by the National Basic Research Program of China (973 Program) under Grant 2011CB707700, the National Natural Science Foundation of China under Grant Nos. 81227901, 61231004, 61363049, the Chinese Academy of Sciences Fellowship for Young International Scientists under Grant 2013Y1GB0005, the National High Technology Research and Development Program of China (863 Program) under 2012AA021105, the "Guangdong Province-Chinese Academy of Sciences" comprehensive strategic cooperation program under 2010A090100032 and 2012B090400039, the NSFC-NIH Biomedical collaborative research program under 81261120414, the Beijing Natural Science Foundation under Grant No. 4132080, the Fundamental Research Funds for the Central Universities under Grant No. 2013JBZ014, the National Basic Research Program of China under Grant No. 61301002 and the Open Project Program of the State Key Laboratory of Management and Control for Complex Systems under Grant No. 20140101.

D. D. Yu and C.Y. Yang are with the Key Laboratory of Molecular Imaging, Institute of Automation, Chinese Academy of Sciences, Beijing 100190, China (e-mail: yudongdongatcasia@gmail.com; caiyang@fingerpass.net.cn).

*F. Yang is with School of Computer and Information Technology, Beijing Jiaotong University, Beijing 100044, China (e-mail: fengyang@bjtu.edu.cn).

C. C. Leng is with the School of Mathematics and Information Sciences, Nanchang Hangkong University, Nanchang 330063, China (e-mail:chengcaileng@gmail.com).

J. Cao and Y. N. Wang are with Department of Radiology, PUMC Hospital, CAMS and PUMC, Beijing 100730, China (e-mail: caojian@pumch.cn; wangyining@pumch.cn).

*J. Tian is with the Key Laboratory of Molecular Imaging, Institute of Automation, Chinese Academy of Sciences, Beijing 100190, China (e-mail: tian@ieee.org).

***Index Terms*—Medical imaging, Rigid image registration, Accelerated NSIFT, Parallel optimization based on Gaussian mixture model, Rotation-free.**

I. Introduction

IMAGE registration is a key problem in a variety of applications of computer vision, medical image processing, pattern recognition, etc. [1]-[3]. It overlays two or more images of the same scene taken at different times, from different viewpoints, and/or by different sensors. Image registration methods are generally classified into two categories: non-feature based registration and feature based registration. Non-feature based registration methods generally use the intensity-based information [4], [5] (the sum of squared or absolute differences, cross correlation, correlation coefficient), attribute-based information [6], [7] (histogram attribute, sobel edge attribute, gabor attribute), or information theory [8]-[10] (mutual information, normalized mutual information, regional mutual information). This kind of approaches has the potential to better quantify and represent the accuracy of the estimated dense deformation field, whereas it comes at the cost of increased computational expense. For feature based registration, salient structures in the images, such as significant regions (forests, lakes, fields), lines (region boundaries, coastlines, roads, rivers) or points (region corners, line intersections, points on curves with high curvature) are firstly extracted as features, and then the solution of the registration problem is converted into matching the extracted features [11]-[13]. Feature based registration is robust with respect to the existence of large deformations. However, extracting reliable features is an open problem and an active topic of research. Feature extraction and feature matching are two main crucial steps for feature based registration due to their determinative effects on algorithm efficiency and robustness [14]. Most existing registration algorithms focus on one of the two steps to improve algorithm performance. In the current study, we focus on the feature based rigid registration particularly on the improvement on feature extraction and feature matching.

The most well-known algorithm for point feature extraction is the Scale Invariant Feature Transform (SIFT) method [15], proposed by Lowe to extract distinctive invariant features from images. SIFT features are invariant to the image scale,

This article has been accepted for publication in a future issue of this journal, but has not been fully edited. Content may change prior to final publication. Citation information: DOI 10.1109/TBME.2015.2465855, IEEE Transactions on Biomedical Engineering

translation and rotation, and provide robust matching across a substantial range of affine distortion, change in 3D viewpoint, addition of noise, and change in illumination. Therefore, it can be used to perform reliable matching between different views of an object or scene. Cheung and Hamarneh [16] extended the SIFT descriptor from 2D scalar images to scalar images of arbitrary dimensionality. This SIFT descriptor is highly discriminant, but being a 128-vector, it is relatively slow in computing and matching. New feature descriptors, such as the GLOH (Gradient location and orientation histogram) descriptor [17], the SURF (Speeded-Up Robust Features) descriptor [18], the DAISY descriptor [19], and the BRIEF descriptor [20], have been proposed either to reduce the descriptor dimension for computation efficiency or to improve the robustness. However, most of these SIFT or SIFT-similar based algorithms assume the one to one correspondence based on the neighbor information of the descriptor, and thus lead to two main effects. On one hand, it costs too much time to describe the interest value; on the other hand, unsatisfactory results may achieve when outliers of the feature description are serious, or when severe deformation or a large pose difference occurs. Note that in this paper, the large pose difference refers to the large rotation between the moving image and the fixed image.

Point set registration, another interesting class of feature based registration, concentrates on feature matching without constructing the descriptor for each interest point but only uses the location information. Mathematically, the point registration problem can be described as: let $\mathbf{M}$ be the moving set with size $n_{\mathbf{M}}$ and $\mathbf{F}$ the fixed set with size $n_{\mathbf{F}}$, in which each element is a vector in $\mathbb{R}^d$, then the task is to find the transformation between the two point sets to yield the best alignment. The iterative closest point (ICP) method [21] is one of the most typical point registration algorithms known for its simplicity in computation and completion. It finds the explicit point correspondence in the two current existing point sets and thus is less sensitive to the missing correspondences and outliers. To deal with the missing correspondences and outliers, some ICP-based algorithms such as BC-ICP [22], Subset-ICP [23], and Dual-Bootstrap ICP [24] have been proposed. However, since the ICP algorithm always converges monotonically to the nearest local minimum of a mean-square distance metric [21], [22], the ICP-based methods would generate significant errors when the moving set and the fixed set are not coarsely aligned. Another category of point registration algorithms models each of the two point sets with a kernel density function [25]-[29] and aligns the density function without establishing the explicit point correspondence. Using the kernel density function, the problem of the point set registration is translated to the density function alignment [25]. Bing *et al* [26], [27] proposed the Gaussian Mixture Model (GMM) registration algorithm, which uses the Gaussian kernel density function as the explicit kernel function to represent the given point sets and aligns the two point sets by aligning the Gaussian Mixture Model. The GMM method is more robust to the missing correspondences and outliers and has been widely used in pattern recognition and medical image analysis, but it may easily fail when the rotation angle between the moving set and the fixed set is large (that is, when the moving and fixed images are of large pose differences) [27]. Based on the analysis above, it can be concluded that a good initial transformation that places the two data sets in approximate registration is required for the point registration algorithms, including ICP based methods and kernel density based algorithms (e.g. GMM method). So far, to our best knowledge, no registration method survives when the rotation is beyond 90 degree.

In this paper, we propose a new feature based rigid registration method which focuses on the improvement of feature extraction and feature matching to reduce the time-consumption and to ameliorate the accuracy in the case of large pose differences. First, an accelerated Multi-dimensional Scale Invariant Feature Transform (A-NSIFT) algorithm is proposed by extracting the interest points from the fixed and moving images using CUDA-programming and preserving only the location information of interest points. Then, the interest point sets extracted by A-NSIFT in both fixed and moving images are represented as Gaussian mixture models, based on which the rigid spatial transformation from the moving set to the fixed set is subsequently calculated by matching the mixture models. In order to solve the registration problem when the fixed and moving images are with large pose differences, we propose a Parallel Optimization based on Gaussian Mixture Model Registration (PO-GMMREG), which can align the moving and fixed images with an arbitrary angle of rotation. It should be noticed that Gaussian Mixture Model Registration is a special case of our registration algorithm. The main contributions of our paper are: (i) extracting feature points using the A-NSIFT method which does not need to construct the feature description of each point but only preserve their location information; (ii) matching the feature points using our PO-GMMREG method, which is proven in both theory and practice working well even in the case of large pose differences.

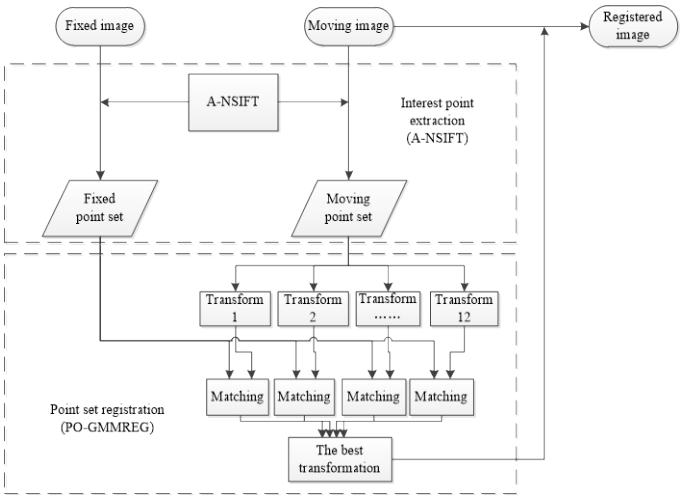

Fig. 1. Flowchart of our fast rotation-free feature based rigid registration algorithm. The two dashed boxes indicate the feature extraction using our proposed A-NSIFT method and feature matching with the PO-GMMREG algorithm respectively.

This article has been accepted for publication in a future issue of this journal, but has not been fully edited. Content may change prior to final publication. Citation information: DOI 10.1109/TBME.2015.2465855, IEEE Transactions on Biomedical Engineering

The rest of the paper is organized as follows. In Section II, we present the main idea of our A-NSIFT method for feature point extraction and our Parallel Optimization based on Gaussian Mixture Model Registration. In Section III are given experimental results and discussion, followed by a conclusion in Section IV.

II. Fast Rotation-Free Feature Based Rigid Registration Framework

The proposed feature based rigid registration algorithm consists of three steps. First, the interest point sets from the fixed and moving images are extracted using our A-NSIFT method, which transforms the image registration into point set registration. Then, a Parallel Optimization based on the Gaussian Mixture Model Registration is proposed in order to obtain the transformation which best matches the fixed point set and moving point set. Finally, the moving image is registered according to the transformation obtained in the second step. The flowchart of our proposed registration algorithm is shown in Fig. 1.

A. Accelerated-NSIFT for interest point extraction

The NSIFT method [16], which extends the SIFT method from 2D to multi-dimensional images, consists of three steps. First, the doG (difference of Gaussian) scale space is constituted by a series of Gaussian blurred images which are generated by a multilevel image pyramid. Then, local feature points are extracted by localizing the extrema in the approximation of doG scale space. Third, the features of each point are depicted by a feature descriptor through summarizing the gradients near this located feature point.

Algorithm 1 The proposed A-NSIFT method based on CUDA-programming

Input: the moving (fixed) image.
Output: the moving (fixed) set
1 **Begin:**
2 load the image in CPU and copy to GPU memory as the initial image $I(v_x, v_y, v_z)$
3 **while** (octavenum<OCTAVE)
4 compute the Gaussian smoothing image series with the initial image $I(v_x, v_y, v_z)$;
5 $L(v_x, v_y, v_z, \sigma) = G(v_x, v_y, v_z, \sigma) * I(v_x, v_y, v_z)$

$$G(v_x, v_y, v_z, \sigma) = \frac{1}{\sqrt{2\pi\sigma^2}^3} e^{-\frac{v_x^2+v_y^2+v_z^2}{2\sigma^2}}$$

6 generate the doG space;
7 $D(v_x, v_y, v_z, \sigma) = L(v_x, v_y, v_z, l\sigma) - L(v_x, v_y, v_z, \sigma)$
8 local the extreme in the doG space, label them in the mask volume and compute the localization.
9 downsample the last scale Gaussian smoothing image in this octave and use it as the initial image.
10 octavenum ++;
11 **endwhile**
12 **End**

Note: OCTAVE indicates the number of down-sampling scales of an image [15].

Feature points extracted from the NSIFT method are invariant to image scale and rotation, whereas it costs too much time to generate the interest points' feature descriptor by the NSIFT method. To reduce the computation cost, we propose an accelerated NSIFT (A-NSIFT) to speed up the NSIFT while extracting the distinctive scale invariant features in the 3D medical image. Our proposed A-NSIFT does not need to construct the feature descriptor, but uses a multilevel image pyramid to generate the doG space and to locate the extrema in the doG space, followed by the acceleration of the first two steps of the NSIFT using CUDA-programming. Algorithm 1 shows the preudocode of our proposed A-NSIFT method, in which the CUDA-programming idea can be found from line 4 to line 9. Four kernels are used in the CUDA-programming: the Gaussian smoothing kernel, the doG generating kernel, the extrema localization kernel and the downsampling kernel.

(1) Gaussian smoothing kernel. This kernel is applied to the initial images (both fixed images and moving images) for the data parallelism by assigning each voxel a thread. Supposing that voxels are stored in the order v_x, v_y, and v_z, then we can use M threads per block and N blocks for all the voxels in data parallelism. Separable filtering and data reuse are integrated into our parallel scheme to speed up the feature extraction. Separable filtering is used to avoid the multi-dimensional convolution and is accomplished by performing convolution of the initial input image with a 3D Gaussian filter. Since the Gaussian filter is separable, the convolution is performed in separate passes for the v_x, v_y, and v_z filters. The second technique is the data reuse using the texture memory, which is completed by allocating texture memory and binding the initial data on it. Since the convolution value at each voxel is correlated with its neighbor voxels, each voxel can be used many times. We would note that the data reuse with the texture memory is also used in the following three steps.

(2) doG generating kernel. This kernel generates the doG space by taking the series of Gaussian blurred images as input and producing the difference of Gaussian space at each voxel respectively in v_x, v_y, *and* v_z directions.

(3) Extrema localization kernel. This group localizes the position of the distinct point. It takes the doG space as the input and label the local extrema in the mask volume.

(4) Downsampling kernel. This kernel downsamples the Gaussian smoothing images. It takes the last scale of Gaussian smoothing image as its input and the downsampled image as the next octave's initial image.

By using our A-NSIFT, interest point sets from both the moving image and the fixed image are extracted, and then the image registration is converted into finding a mapping from the two interest point sets.

B. Parallel optimization based on GMM registration

1) Point set registration with the Gaussian mixture model

Based on the interest point extraction, the moving point set can be obtained as well as the fixed set, in which each point can be treated as a statistical sample from a continuous probability distribution. Thus, the probability distribution (which is a continuous density function) of the interest point set can be represented by a Gaussian mixture model [30], [31] as

This article has been accepted for publication in a future issue of this journal, but has not been fully edited. Content may change prior to final publication. Citation information: DOI 10.1109/TBME.2015.2465855, IEEE Transactions on Biomedical Engineering

$$\begin{cases} p(x) = \sum_{i=1}^{k} \omega_i \phi(x \mid \boldsymbol{\mu}_i, \boldsymbol{\Sigma}_i) \\ \phi(x \mid \boldsymbol{\mu}_i, \boldsymbol{\Sigma}_i) = \dfrac{\exp(-\dfrac{(x-\boldsymbol{\mu}_i)^T \boldsymbol{\Sigma}_i^{-1}(x-\boldsymbol{\mu}_i)}{2})}{\sqrt{(2\pi)^d \det(\boldsymbol{\Sigma}_i)}} \end{cases}, \quad (1)$$

where, $\phi(x \mid \boldsymbol{\mu}_i, \boldsymbol{\Sigma}_i)$ indicates the i^{th} component of a Gaussian mixture model, $\boldsymbol{\mu}_i$ corresponds to the mean vector of the i^{th} component, $\boldsymbol{\Sigma}_i$ denotes the covariance matrix of the i^{th} component, ω_i is the weight of the i^{th} component and k is the number of Gaussian mixture model components.

In (1) each component of the Gaussian mixture model is a cluster and may contain several points of the interest point set. For simplification, each point in the interest point set can be treated as a cluster or a component of the Gaussian mixture model. Kanazawa and Kanatani [32] have demonstrated by experiments that this simplification has no significant effect on the results of image registration. In this case, the mean vector of each component is the value in this point, and the covariance matrix is different from the identity matrix by a fixed scale factor. Therefore, both the moving set and the fixed set are represented as a Gaussian mixture model,

$$gmm(\mathbf{M}) = \sum_{i=1}^{n_M} \alpha_i \phi(x \mid \boldsymbol{\mu}_i, \boldsymbol{\Sigma}_i), \quad (2)$$

$$gmm(\mathbf{F}) = \sum_{j=1}^{n_F} \beta_j \phi(x \mid \boldsymbol{\xi}_j, \boldsymbol{\Gamma}_j). \quad (3)$$

The problem of interest point set registration is now translated into the alignment of Gaussian mixture models. This alignment can be solved by optimizing the cost function that measures the similarity between $gmm(\mathbf{M})$ and $gmm(\mathbf{F})$. A distance metric based on the L_2 divergence is used as the cost function to measure the similarity of Gaussian mixture models

$$d_{L_2}(\mathbf{M}, \mathbf{F}, \boldsymbol{\theta}) = \int (gmm(\mathbf{F}) - gmm(T(\mathbf{M}, \boldsymbol{\theta})))^2 dx, \quad (4)$$

where, $T(\mathbf{M}, \boldsymbol{\theta})$ indicates the registered point set when applying a transformation T to the moving set $\mathbf{M}$, and $\boldsymbol{\theta}$ is a vector of the transformation parameters which include rotation and translation for rigid registration but correspond to the coefficients in interpolation algorithms for non-rigid registration. The image registration is then to find the parameter vector $\boldsymbol{\theta}$ of transformation T to minimize the cost function.

In this paper, we apply the Gaussian mixture model alignment for rigid registration but will ameliorate its performance in the case of large pose differences (see the II (2) subsection). Since a rigid transformation can be characterized by a rotation matrix $\mathbf{R}$ and a translation vector $\mathbf{t}$, the transformation parameter vector $\boldsymbol{\theta}$ is determined by $\mathbf{R}$ and $\mathbf{t}$. In this study, we use a quaternion $\mathbf{q} = (r_1, r_2, r_3, r_4)^T$ to represent the 3D rotation $\mathbf{R}$ for its simplicity and its stable property in 3D space. A 3D rotation $\mathbf{R}$ can be obtained from $\mathbf{q}$ by

$$\mathbf{R} = \begin{pmatrix} r_4^2 + r_1^2 - r_2^2 - r_3^2 & 2(r_1 r_2 + r_3 r_4) & 2(r_3 r_1 - r_4 r_2) \\ 2(r_1 r_2 - r_3 r_4) & r_4^2 - r_1^2 + r_2^2 - r_3^2 & 2(r_2 r_3 + r_1 r_4) \\ 2(r_1 r_3 + r_2 r_4) & 2(r_2 r_3 - r_1 r_4) & r_4^2 - r_1^2 - r_2^2 + r_3^2 \end{pmatrix}. \quad (5)$$

Denoting the translation as $\mathbf{t} = (t_1, t_2, t_3)^T$, then $\boldsymbol{\theta}$ can be defined as $\boldsymbol{\theta} = (r_1, r_2, r_3, r_4, t_1, t_2, t_3)^T$. When applying a rigid registration to the moving set $\mathbf{M}$, the Gaussian mixture model of the registered point set can be derived as

$$gmm(T(\mathbf{M}, \boldsymbol{\theta})) = \sum_{i=1}^{n_M} \alpha_i \phi(x \mid \mathbf{R}\boldsymbol{\mu}_i + \mathbf{t}, \mathbf{R}\boldsymbol{\Sigma}_i \mathbf{R}^T). \quad (6)$$

By applying (2), (3) and (6) to (4), our cost function $d_{L_2}(\mathbf{M}, \mathbf{F}, \boldsymbol{\theta})$ then can be expressed as

$$\begin{aligned} & d_{L_2}(\mathbf{M}, \mathbf{F}, \boldsymbol{\theta}) = \\ & \int gmm(\mathbf{F})^2 - 2gmm(\mathbf{F})gmm(T(\mathbf{M}, \boldsymbol{\theta})) + gmm(T(\mathbf{M}, \boldsymbol{\theta}))^2 dx \\ & = \sum_{i=1}^{n_F} \sum_{j=1}^{n_F} \beta_i \beta_j \phi(0 \mid \boldsymbol{\xi}_i - \boldsymbol{\xi}_j, \boldsymbol{\Gamma}_i + \boldsymbol{\Gamma}_j) + \\ & \sum_{i=1}^{n_M} \sum_{j=1}^{n_M} \alpha_i \alpha_j \phi(0 \mid \mathbf{R}\boldsymbol{\mu}_i - \mathbf{R}\boldsymbol{\mu}_j, \mathbf{R}(\boldsymbol{\Sigma}_i + \boldsymbol{\Sigma}_j)\mathbf{R}^T) - \\ & 2\sum_{i=1}^{n_F} \sum_{j=1}^{n_M} \beta_i \alpha_j \phi(0 \mid \boldsymbol{\xi}_i - \mathbf{R}\boldsymbol{\mu}_j - \mathbf{t}, \boldsymbol{\Gamma}_i + \mathbf{R}\boldsymbol{\Sigma}_j \mathbf{R}^T) \end{aligned} \quad (7)$$

The registration problem now comes to the optimization problem of $Min\, d_{L_2}(\mathbf{M}, \mathbf{F}, \boldsymbol{\theta})$. The alignment of Gaussian mixture models can avoid establishing the explicit point correspondence, and thus is more robust to the missing or fault correspondences. In addition, by using continuous function to represent discrete point sets, the continuous optimization can be used to solve the cost function, which will improve the efficiency and simplicity of the matching algorithms. Generally, the ranges of the rotation and translation vary greatly, and to reduce this variation, a normalization of the moving set and the fixed set will be performed before the Gaussian mixture matching. A normalization of the moving set and the fixed set could be performed as: $\mathbf{m}' = (\mathbf{m} - \mathbf{centroid\_m})/scale\_m$ and $\mathbf{f}' = (\mathbf{f} - \mathbf{centroid\_f})/scale\_f$, where $\mathbf{m}$ and $\mathbf{f}$ respectively denote the moving point set and the fixed point set, $\mathbf{centroid\_m}$ and $\mathbf{centroid\_f}$ represent the geometric center of the moving and fixed sets, and $scale\_m$ and $scale\_f$ are the frobenius norms of the corresponding point sets.

2) Parallel Optimization

As mentioned above, we align the Gaussian mixture model to match the moving and fixed point sets which are extracted by the A-NSIFT, however, unfortunately, the registration results are not satisfactory when the large pose difference occurs between the two images. Lots of experiments show that the Gaussian mixture matching works well when the rotation of angle θ about an arbitrary axis is less than 90 degree, but does not function well any more when θ is beyond 90 degree. In order to deal with this problem, we propose a new algorithm PO-GMMREG based on the Gaussian mixture model matching, which could deal with the case of large pose difference (rotation angle larger than 90 degree).

The key point of our algorithm is to find an initial spatial transformation set to ensure the rotation between the new moving set (the transformed point set from the moving set using the initial transformation) and the fixed set is less than 90 degree. We first constructed an initial spatial transformation set represented by 12 quaternions

This article has been accepted for publication in a future issue of this journal, but has not been fully edited. Content may change prior to final publication. Citation information: DOI 10.1109/TBME.2015.2465855, IEEE Transactions on Biomedical Engineering

$\mathbf{\Omega}=\{(1,0,0,0)^T,(0,1,0,0)^T,(0,0,1,0)^T,(0,0,0,1)^T,$
$(\frac{1}{2},\frac{1}{2},\frac{1}{2},\frac{1}{2})^T,(-\frac{1}{2},\frac{1}{2},\frac{1}{2},\frac{1}{2})^T,(\frac{1}{2},-\frac{1}{2},\frac{1}{2},\frac{1}{2})^T,(-\frac{1}{2},-\frac{1}{2},-\frac{1}{2},\frac{1}{2})^T,$
$(-\frac{1}{2},\frac{1}{2},-\frac{1}{2},\frac{1}{2})^T,(\frac{1}{2},-\frac{1}{2},-\frac{1}{2},\frac{1}{2})^T,(\frac{1}{2},\frac{1}{2},-\frac{1}{2},\frac{1}{2})^T,(-\frac{1}{2},-\frac{1}{2},\frac{1}{2},\frac{1}{2})^T\}$,

which is proven to be able to guarantee the rotation angle between the new moving and the fixed sets less than 90 degree. The problem of constructing the initial spatial transformation set $\mathbf{\Omega}$ is shown in Fig.2 and reformulated in (8), in which $\mathbf{F},\mathbf{M},\mathbf{Tr}$ respectively indicate the fixed point set, moving point set and transformed point set (or the new moving point set) and $\Theta(,)$ is the rotation computation operator to calculate the angle between two point sets. T is a spatial transformation represented by a quaternion that transforms the moving point set to the transformed set. All the transformations that satisfy (8) compose the initial spatial transformation set $\mathbf{\Omega}$, which is composed by the twelve quaternions above

$$\begin{cases} \textit{Construct } \mathbf{\Omega}, \textit{ s.t.} -\frac{\pi}{2} \le \Theta(\mathbf{F},\mathbf{Tr}) \le \frac{\pi}{2} \\ \mathbf{Tr} = T \circ \mathbf{M},\ T \in \mathbf{\Omega} \\ -\pi \le \Theta(\mathbf{F},\mathbf{M}) \le \pi \end{cases} . \quad (8)$$

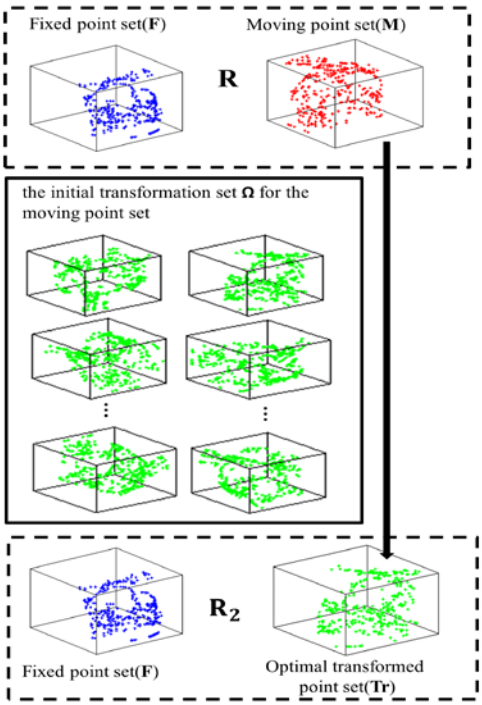

Fig. 2. Reformulation of the initialization problem. **R** indicates the rotation between the moving point set and the fixed point set, while the corresponding rotation angle is between –π and π. $\mathbf{R_2}$ represents the rotation between the optimal transformed point set and the fixed point set, and its corresponding rotation angle is between –π/2 and π/2. Our objective is to find the optimal transformation from our constructed 12-quaternion set to obtained the optimal transformed point set.

Proposition: If we have two point sets, fixed point set $\mathbf{F}$, moving point set $\mathbf{M}$, a rotation $\mathbf{R}$ is needed to register the moving point set to the fixed point set $\mathbf{F}$. The rotation angle α_{real} (corresponding to $\mathbf{R}$) is $(-\pi,\pi]$. The initialization process is to find a transformation $q_{initial}$ to transform the moving point set $\mathbf{F}$ to the transformed point set $\mathbf{Tr}$. We construct a quaternion transformation set $\mathbf{\Omega}$, in which there exists at least one quaternion transformation which can guarantee the rotation angle α (corresponding to $\mathbf{R}_2$) between the fixed set $\mathbf{F}$ and the transform set $\mathbf{Tr}$ to be $(-\frac{\pi}{2},\frac{\pi}{2}]$.

Proof: Let $\mathbf{m},\mathbf{f},\mathbf{m}',\mathbf{f}',\mathbf{p}'$ respectively represent the moving point set, the fixed point set, the normalized moving set, the normalized fixed set and the transformed set. Let $\mathbf{R}_1,\mathbf{R}_2,\mathbf{R}_{real}$ denote the rotation matrix between the normalized moving set and the transformed set, the rotation between the transformed set and the normalized fixed set, and the rotation between the normalized fixed and the normalized moving set, respectively. Then the rotation between the normalized fixed set and the normalized moving set can be calculated by combining the rotation between the normalized moving set and the transformed set and the rotation between the transformed set and the normalized fixed set by $\mathbf{R}_{real}=\mathbf{R}_2\mathbf{R}_1$. Since the rotation matrix can be represented by quaternions, we use $\mathbf{q}_{initial}=(q_{initial,0},q_{initial,1},q_{initial,2},q_{initial,3})^T$, $\mathbf{q}_{compute}=(q_{compute,0},q_{compute,1},q_{compute,2},q_{compute,3})^T$ and $\mathbf{q}_{\text{real}}=(q_{\text{real},0},q_{\text{real},1},q_{\text{real},2},q_{\text{real},3})^T$ to indicate the unit quaternion corresponding to rotation $\mathbf{R}_1$, $\mathbf{R}_2$ and $\mathbf{R}_{real}$, respectively. Then, we can get $\mathbf{q}_{real}=\mathbf{q}_{compute}\mathbf{q}_{initial}$. A quaternion can also be represented as $\mathbf{q}=\left(\sin\frac{\alpha}{2}\omega_x,\sin\frac{\alpha}{2}\omega_y,\sin\frac{\alpha}{2}\omega_z,\cos\frac{\alpha}{2}\right)^T$, which geometrically corresponds to a rotation about an arbitrary axis $\varpi=(\omega_x,\omega_y,\omega_z)^T$ with an angle α. Therefore, to prove that the rotation of angle θ about an arbitrary axis (through the origin) is less than 90 degree between the transformed set and the fixed set, we just need to prove the rotation angle represented by $\mathbf{q}_{compute}$ is less than 90 degree, that is $|q_{compute,3}|\ge\cos\frac{90°}{2}=\frac{\sqrt{2}}{2}$. Based on the notation above, we can get $\mathbf{q}_{compute}=\mathbf{q}_{real}\mathbf{q}_{initial}^{-1}$, where $\mathbf{q}_{initial}^{-1}=(q_{initial,0}^{-1},q_{initial,1}^{-1},q_{initial,2}^{-1},q_{initial,3}^{-1})^T$ is the inverse of $\mathbf{q}_{initial}$. Therefore, the $|q_{compute,3}|$ can be calculated as

$$|q_{compute,3}|=|q_{real,0}q_{initial,0}^{-1}-q_{real,1}q_{initial,1}^{-1}-q_{real,2}q_{initial,2}^{-1}-q_{real,3}q_{initial,3}^{-1}|. \quad (9)$$

To ensure that, with our constructed initial transformation set $\mathbf{\Omega}$, the rotation angle between the new moving set (or the transformed set) and the fixed set is less than 90 degree, we just need to guarantee $|q_{compute,3}|\ge\frac{\sqrt{2}}{2}$.

This article has been accepted for publication in a future issue of this journal, but has not been fully edited. Content may change prior to final publication. Citation information: DOI 10.1109/TBME.2015.2465855, IEEE Transactions on Biomedical Engineering

Assuming that $q_{real,0} \ge 0, q_{real,1} \ge 0, q_{real,2} \ge 0, q_{real,3} \ge 0$, for a unit quaternion, there always exists one of the following five formulas (a) (b) (c) (d) (e) in (10) which is tenable.

$$\begin{cases} q_{real,1} * 1 + q_{real,1} * 0 + q_{real,2} * 0 + q_{real,3} * 0 \ge \dfrac{\sqrt{2}}{2} & (a) \\ q_{real,1} * 0 + q_{real,1} * 1 + q_{real,2} * 0 + q_{real,3} * 0 \ge \dfrac{\sqrt{2}}{2} & (b) \\ q_{real,1} * 0 + q_{real,1} * 0 + q_{real,2} * 1 + q_{real,3} * 0 \ge \dfrac{\sqrt{2}}{2} & (c) \\ q_{real,1} * 0 + q_{real,1} * 0 + q_{real,2} * 0 + q_{real,3} * 1 \ge \dfrac{\sqrt{2}}{2} & (d) \\ q_{real,1} * \dfrac{1}{2} + q_{real,1} * \dfrac{1}{2} + q_{real,2} * \dfrac{1}{2} + q_{real,3} * \dfrac{1}{2} \ge \dfrac{\sqrt{2}}{2} & (e) \end{cases} . \quad (10)$$

For example, if one of the formulae (*a*)-(*d*) is correct, $\mathbf{q}_{initial}^{-1}$ can be chosen as one of $\{(1,0,0,0)^T, (0,1,0,0)^T, (0,0,1,0)^T, (0,0,0,1)^T\}$, then we can easily obtain

$$| q_{real,0} q_{initial,0}^{-1} - q_{real,1} q_{initial,1}^{-1} - q_{real,2} q_{initial,2}^{-1} - q_{real,3} q_{initial,3}^{-1} | \ge \frac{\sqrt{2}}{2}. \quad (11)$$

If (*a*) (*b*) (*c*) (*d*) are all incorrect, then there exists $q_{real,0} < \frac{\sqrt{2}}{2}, q_{real,1} < \frac{\sqrt{2}}{2}, q_{real,2} < \frac{\sqrt{2}}{2}, q_{real,3} < \frac{\sqrt{2}}{2}$. Since $q_{real,0}^2 + q_{real,1}^2 + q_{real,2}^2 + q_{real,3}^2 = 1$, one can readily obtain (*e*). In this situation, $\mathbf{q}_{initial}^{-1}$ can be chosen as one of

$\{(\frac{1}{2},\frac{1}{2},\frac{1}{2},\frac{1}{2})^T, (-\frac{1}{2},\frac{1}{2},\frac{1}{2},\frac{1}{2})^T, (\frac{1}{2},-\frac{1}{2},\frac{1}{2},\frac{1}{2})^T, (\frac{1}{2},\frac{1}{2},-\frac{1}{2},\frac{1}{2})^T,$

$(-\frac{1}{2},\frac{1}{2},-\frac{1}{2},\frac{1}{2})^T, (\frac{1}{2},-\frac{1}{2},-\frac{1}{2},\frac{1}{2})^T, (-\frac{1}{2},-\frac{1}{2},-\frac{1}{2},\frac{1}{2})^T, (-\frac{1}{2},-\frac{1}{2},\frac{1}{2},\frac{1}{2})^T\}$,

and then we can get the inequation (11).

It follows that there exists at least one point set in the twelve transformed sets which can guarantee the rotation angle between the transformed set and the fixed set less than 90 degree.

The proof can be performed similarly in other 15 cases besides $q_{real,0} \ge 0, q_{real,1} \ge 0, q_{real,2} \ge 0, q_{real,3} \ge 0$. ■

Based on GMMREG algorithm, the cost function optimization of our proposed PO-GMMREG can be represented as

$$\begin{cases} Min_i Min \ \ d_{L_2}(\mathbf{M}, \mathbf{F}, \boldsymbol{\theta}, \mathbf{q}_{initial,i}) \\ \boldsymbol{\theta} = (r_1, r_2, r_3, r_4, t_1, t_2, t_3)^T \\ \mathbf{q} = (r_1, r_2, r_3, r_4)^T \\ \mathbf{t} = (t_1, t_2, t_3)^T \\ \mathbf{q}_{initial,i} \in \Omega \\ \mathbf{R} = \mathbf{R}_2 \mathbf{R}_1 \end{cases} . \quad (12)$$

Then, our PO-GMMREG algorithm can be completed by the steps shown in Algorithm 2.

Algorithm 2. Outline of our parallel optimization algorithm based on Gaussian mixture model registration.

Input: the moving image, the fixed image and an initial parameterized rigid transformation $\boldsymbol{\theta}$.

Output: the matched image and the optimal transformation between the moving image and the fixed image.

1 **Begin:**
2 use the A-NSIFT on the moving image and fixed image, and get the interest point set called the moving set $\mathbf{M}$, the fixed set $\mathbf{F}$.
3 normalize the $\mathbf{M}, \mathbf{F}$, and get the normalized moving set $\mathbf{M}'$, the normalized fixed set $\mathbf{F}'$.
4 **foreach(quaternion in Ω)**
5 use the quaternion to rotate the normalized moving set $\mathbf{M}'$, then get the middle set $\mathbf{M}''$
6 estimate an initial scale σ from the $\mathbf{M}''$ and $\mathbf{F}'$, specify an initial parameter $\boldsymbol{\theta}$ of a rigid registration.
7 **repeat:**
Set up the cost function $f(\boldsymbol{\theta})$ as the L_2 distance between the Gaussian mixtures constructed from the transformed middle set $\mathbf{M}''$ and the normalized fixed set $\mathbf{F}'$.
8 optimize the cost function f using a numerical optimization engine, with $\boldsymbol{\theta}$.
9 update $\boldsymbol{\theta} \leftarrow \arg\min_{\boldsymbol{\theta}} f$
10 decrease the scale σ as an annealing step
11 **until** some stopping criterion is satisfied
12 **endforeach**
13 find the min in all $\arg\min_{\boldsymbol{\theta}} f$
14 update $\boldsymbol{\theta} \leftarrow \min \arg\min_{\boldsymbol{\theta}} f$
15 compute the rigid registration from $\boldsymbol{\theta}$ and the mapping **quaternion**.
16 transform the moving image with the rigid registration, then get the matched image.
17 **END**

III. Experimental Results and Discussion

To evaluate the performance of our fast rotation-free feature based rigid registration algorithm, experiments are performed on range data from Stanford 3D scanning repository (http://graphics.stanford.edu/data/3Dscanrep/), real medical images downloaded from Kitware (http://public.kitware.com/pub/itk/Data/BrainWeb/) and RIRE (http://www.insight-journal.org/rire/download.php), and clinical cardiac diffusion tensor MRI (DTMRI) data from Peking Union Medical College Hospital.

Range data: the range data concerns two categories of 3D scanning range data with a range of different poses, including the "bunny" range data set and the "dragon" range data sets [27,33,36]. For the "bunny" range data, two subsampled models of 4100×3 points with 45 degree rotation angle difference in pose were used for algorithm performance evaluation. For the "dragon" range data, 15 subsampled models of 2500×3 points with in-plane rotation angles from 0 to 336 degree evenly spaced by 24 degrees were used.

Real brain MRI data: the real data sets contains 6 groups of PD-MR, T1-MR and T2-MR images with different rotation angles and translation and 18 groups PD-MR images with artificial rotations from 0 to 180 degree with the same

This article has been accepted for publication in a future issue of this journal, but has not been fully edited. Content may change prior to final publication. Citation information: DOI 10.1109/TBME.2015.2465855, IEEE Transactions on Biomedical Engineering

resolution 1mm×1mm×1mm.

Clinical Cardiac DTMRI data: five formalin-fixed healthy human heart samples were acquired at room temperature on a Siemens 3.0T MAGNETOM Skyra MR scanner in Peking Union Medical College Hospital, with the acquisition parameters as: TE=67 ms, TR=6500 ms, FOV=200× 200 mm, slice thickness= 2.0 mm, number of slices=40~45, 100×100 pixels for each slice, diffusion sensitivity b=1000 s/mm^2, accel factor=2, gradient directions=20, slice gap=0 mm. Total image acquisition time was about 20 min per sample. Since these hearts were acquired ex-vivo, the position and orientation of each sample would have large difference. In our experiment, we focus on the b0 image registration, which is the basis of other diffusion weighted image registration or the registration of corresponding diffusion tensor fields [34].

Performance evaluation: the performance of the proposed registration algorithm were qualitatively and quantitatively assessed using the convergence range, the capability to handle the large pose differences, the computation cost, the accuracy of registration, 3D visualization, etc.. Four registration methods were used in this paper: LM-ICP [35], CPD [36], GMM [27] and our proposed algorithm.

To evaluate the convergence range of the proposed registration algorithm, "dragonStandRight_72" was selected and rotated from 0 to 2π, and the rotated data sets were then registered to the "dragonStandRight_72" using different registration methods. Then the Stanford "dragon stand" data sets were selected to evaluate the performance of these algorithms to handle the large pose differences. The registration accuracy of a 3D rotation is evaluated by first representing rotations in unit quaternions and then taking the absolute value of the dot product between the two unit quaternions. The closer this dot product is to 1, the more accurate the 3D registration is. If the accuracy value is greater than 0.99, we say this registration is successful, and then the success rate can be calculated by the ratio of the number of successful registrations and the total number of registration.

To evaluate the speed and the computation cost of our registration algorithm, 6 groups of real medical images were used to compare our proposed method with the conventional NSIFT method, the conventional GMM method and ICP algorithm. In order to demonstrate the accuracy of our registration algorithm, the registration error generated by A-NSIFT-GMM registration, A-NSIFT-ICP registration, and

(a) (b) (c)

Fig. 3. Qualitative registration results of our proposed method on Stanford "bunny" range data. (a) and (b) correspond to the Stanford "bun000" model and "bun045" model, respectively. (c) is the transformed "bun000" using the 3D rigid motion obtained with our proposed registration algorithm. Each model consists of a large number of points, and the color from dark to white indicates the brightness of the figure, which reflects the points scanned from this model. The brighter the figure is, the less the density of the point is. Since the "bun000" model and "bun045" model were rotated first in different poses and then scanned to images, the distributions of the points are different, and thus their brightness are different.

(a) (b) (c) (d)

Fig. 4. Qualitative registration results on Stanford "dragon" range data. (a) and (b) indicate the Stanford "dragonStandRight_144" model and "dragonStandRight_240" model, respectively. (c) and (d) are the transformed "dragonStandRight_240" using the 3D rigid motion obtained from the GMM algorithm and our proposed registration algorithm, respectively.

(a) (b) (c) (d)

Fig. 5. Qualitative registration results on Stanford "dragon" range data. (a) and (b) are the Stanford "dragonStandRight_216" model and "dragonStandRight_312" model, respectively. (c) and (d) demonstrate the transformed "dragonStandRight_312" using the 3D rigid motion obtained from the GMM algorithm and our proposed registration algorithm, respectively.

This article has been accepted for publication in a future issue of this journal, but has not been fully edited. Content may change prior to final publication. Citation information: DOI 10.1109/TBME.2015.2465855, IEEE Transactions on Biomedical Engineering

our registration method was calculated, which is defined as

$$\varepsilon = \frac{\sum_{i=1}^{8} \| T_{real}(v_i) - T(v_i) \|}{8}, \quad (13)$$

where $T(\bullet)$ indicates the transformation calculated with different methods, $T_{real}(\bullet)$ denotes the real transformation between the moving image and fixed image, and v_i (i=1,2…8) is the eight vertices of a 3D image. Since the error in the vertices is the biggest among all of the voxels, it is reasonable to measure the registration error in the eight vertices.

All of the experiments were performed on a PC with 6GB of RAM, 3.07GHz Intel CPU and a graphics card NVIDIA Geforce GTX 480.

A. *Range data*

Fig. 3 shows the results of registration between two 3D range scan data sets with 45 degree rotation difference in pose. The "bun000" model and "bun045" model were scanned from the same bunny while the laser scanner was rotated 45 degree about a 3D axis. The CPD registration algorithm, the LM-ICP registration algorithm, the GMM registration algorithm and our proposed PO-GMMREG method were used to align the "bun000" model to the "bun045" model. It is observed that all the four algorithms achieve the registration successfully, and only the result using the proposed algorithm is shown in Fig. 3.

In Fig. 6 are plotted the registration errors of the convergence range when using the CPD registration, the LM-ICP registration, the GMM registration and our proposed PO-GMMREG method to register "dragonStandRight_72" to the original one with respect to different rotation angles from 0 to 2π. It is observed that CPD and GMM algorithms perform well when the initial rotation (degrees) of initial misalignment is less than 90 degree, whereas ICP gets trapped into a local minimum with rotations beyond 60 degree. In contrast, our proposed algorithm can work well no matter how large the rotation difference is.

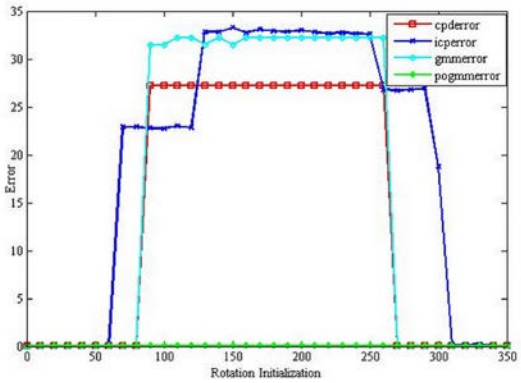

Fig. 6. Profile of registration errors with respect to the initial rotation (degrees) differences in pose using the four methods.

In order to quantitatively evaluate the performance of these algorithms with respect to the pose differences, we chose the Stanford "dragon stand" data set, which contains 15 scans with in- plane rotation angles from 0 to 336 degree evenly spaced by 24 degrees. Experiments were conducted on each 30 pairs with different ration angles. In Table I are summarized the success rates when using the four registration methods on the pairs with pose difference being ± 24, ± 48, ± 72, and ± 96 degree, respectively. According to the results, all of these four algorithms achieve good performance when the pose difference between the 3D scans is less than 72 degree. However, when the pose difference is larger than 72 degree, GMM, CPD, and LM-ICP exhibit a poor success rate, which could be obviously well improved by the proposed method.

TABLE I
SUCCESS RATES OF OUR PROPOSED REGISTRATION ALGORITHM, THE GMM ALGORITHM, THE CPD ALGORITHM AND THE LM-ICP ALGORITHM ON THE STANFORD "DRAGON STAND" DATA SET

Pose difference	Our method	GMM	CPD	LM-ICP
±24° [0.978]	30/30	29/30	26/30	28/30
±48° [0.913]	24/30	20/30	18/30	19/30
±72° [0.809]	16/30	13/30	14/30	13/30
±96° [0.669]	12/30	2/30	3/30	1/30

In fact, we also did the same experiments using the proposed method for the pairs with the pose difference respectively being ± 120, ± 144, and ± 168 degree, and the success rates are 8/30, 9/30, and 16/30, separately. The registration success rates of GMM, CPD, and LM-ICP algorithms are almost zero in such situations. It is observed that the success rate of our proposed method is still low for the large pose difference cases, which is due to two main reasons. First, the fixed model and the moving model of "Dragon" data with large different pose have original significant different appearances. Second, we downsampled both the fixed and moving model from the original one more than 20000 points to 2000-3000 points using the random down-sample scheme, which may result in uncorrelated point pairs. In Fig. 4 are shown the registration results using the proposed method and the GMM method with the "dragonStandRight_144" model and "dragonStandRight_240" model that have significant outliers respectively chosen as the fixed and moving models. We can see that both the proposed method and GMM method failed. We performed the similar experiment with the "dragonStandRight_216" model and "dragonStandRight_312" model (see Fig. 5). We can see that the GMM method failed to align them, whereas our method can register them well. From the convergence range experiments and pose difference experiments, we can conclude that our proposed method performs well even when the rotation angle is large, however, when the outliers and unrelated point pairs are significant in the fixed and moving models, our proposed method may not work well as other algorithms.

B. *Real brain medical data*

Experiments on the computation cost of point extraction with the conventional NSIFT algorithm and our method are performed on real brain medical datasets PD-MR, T1-MR and T2-MR. Image information and the average computation time of each algorithm are listed in Table II. It is observed in Table II that the extraction of interest points is obviously accelerated by our proposed A-NSIFT method with an accelerated rate more than 200 compared to the conventional NSIFT algorithm. The

This article has been accepted for publication in a future issue of this journal, but has not been fully edited. Content may change prior to final publication. Citation information: DOI 10.1109/TBME.2015.2465855, IEEE Transactions on Biomedical Engineering

acceleration is due to the CUDA-programming and the replacement of constructing the interest points' descriptor by only preserving location information.

TABLE II
AVERAGE COMPUTATION TIME FOR INTEREST POINT EXTRACTION WITH THE CONVENTIONAL NSIFT AND OUR A-NSIFT ALGORITHMS. THE LAST COLUMN IS THE ACCELERATION RATE

Image size	NSIFT	A-NSIFT	Acceleration rate[a]
181×217×180	1307547ms	5165ms	253x
256×256×26	391578ms	1534ms	255x
256×256×128	1153358ms	5258ms	219x

[a] Note: the acceleration rate is obtained by dividing the computation time of NSIFT by that of A-NSIFT.

To evaluate the speed of our point registration algorithm PO-GMMREG, we compare the registration time using three matching methods ICP, GMM and our PO-GMMREG but all combined with the same point extraction algorithm A-NSIFT for the three datasets. Each dataset has two groups of moving images and fixed images. In the first group, the rigid transformation between the moving image and the fixed image is 10° on rotation and 15mm on translation. In the second group the rigid transformation is 20° on rotation and 20mm on translation. The computation time of each group for the three datasets is given in Table III.

It is noted in Table III that our method is much faster than the A-NSIFT-ICP method, but slower than the A-NSIFT-GMM method. In the six group experiments, the average computation time of the NSIFT-ICP method, the NSIFT-GMM method and our method are 34.086s, 9.148s and 13.406s respectively. The GMM is a special case of our PO-GMMREG algorithm, whereas our algorithm manages to solve the problem of image registration with an arbitrary rotation at the price of more computation.

TABLE III
COMPUTATION TIME OF 3D IMAGE REGISTRATION RESPECTIVELY BY A-NSIFT-ICP, A-NSIFT-GMM, AND OUR A-NSIFT-PO-GMM METHODS. THE FIRST COLUMN INDICATES THE IMAGE MODALITY, AND THE LAST THREE COLUMNS SHOW THE COMPUTATION TIME WITH THE THREE DIFFERENT METHODS

		A-NSIFT-ICP	A-NSIFT-GMM	Our method
PD-MR	group1	36453ms	9188ms	16297ms
	group2	42704ms	9328ms	14156ms
T1-MR	group1	14250ms	8750ms	9813ms
	group2	26172ms	8782ms	9656ms
T2-MR	group1	38313ms	9281ms	15000ms
	group2	46625ms	9563ms	15515ms

Evaluation of the performance with respect to the pose difference (i.e. the rotation between the two images) is also performed on the PD-MR brain images with in-plane rotation angles from 10° to 180° which are evenly spaced by 10°. If the registration error is less than 5mm, the result is recorded. The registration error with different methods and different rotations is shown in Fig. 7. It is observed that the error of our method is much smaller than those of the A-NSIFT-ICP and A-NSIFT-GMM methods. In all the experiments, the error of our method is less than 0.6mm and the average registration error is 0.16mm. The average error of the A-NSIFT-ICP method is 1.51mm and the average error of the A-NSIF-GMM method is 0.18mm. It should be noticed that both A-NSIFT-ICP and A-NSIFT-GMM fail to register the images when a large pose difference (rotation larger than 60° for the ICP method and larger than 90° for the GMM method) emerges. Moreover, the registration error of our proposed method can be maintained at a low level. Since the A-NSIFT-GMM algorithm is a special case of our algorithm, it is not surprising that the error is the same when the rotation degree is less than 90°.

In order to visually demonstrate the performances of different registration methods with real brain data, experimental results are shown in Figs. 8-10 for the PD-MR dataset with the A-NSIFT-ICP method, A-NSIFT-GMM method and our method when the rotation angles between the fixed image and moving image are 60°, 90° and 120° respectively. We use the chessboard difference evaluation method which combines two images in a checkerboard pattern by alternating the blocks with the corresponding pixels of the two images to visualize the difference between the fixed image and the registered image.

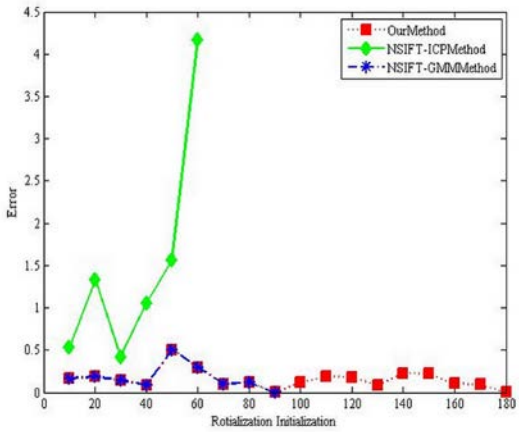

Fig. 7. The registration error using A-NSIFT-ICP, A-NSIFT-GMM and our method on the PD-MR brain image dataset with in-plane rotation angles varying from 10° to 180° which are evenly spaced by 10°.

From Fig. 8(c), we can see that the fixed image and the moving image have substantial difference. From Fig. 8(d)-(f), it is observed that the images are visually well registered using A-NSIFT-ICP, A-NSIFT-GMM and our method, which can be validated by results in Fig. 8(g)-(i) that the fixed image and the three registered image's chessboard differences with the three methods are all small when the rotation is 60°.

Substantial chessboard differences between the registered image and the fixed image have been observed in Fig.9(g), which implies that the A-NSIFT-ICP does not function well in the case of 90° rotation. In contrast, the chessboard differences of the A-NSIFT-GMM and our method are small in the case of 90° rotation shown in Fig. 9(h) and (i).

It is observed in Fig. 10(g) and (h) that, when the rotation angle is up to 120°, both A-NSIFT-ICP and A-NSIFT-GMM generate substantial chessboard differences, whereas almost few difference is produced by our method shown in Fig. 10(i).

This article has been accepted for publication in a future issue of this journal, but has not been fully edited. Content may change prior to final publication. Citation information: DOI 10.1109/TBME.2015.2465855, IEEE Transactions on Biomedical Engineering

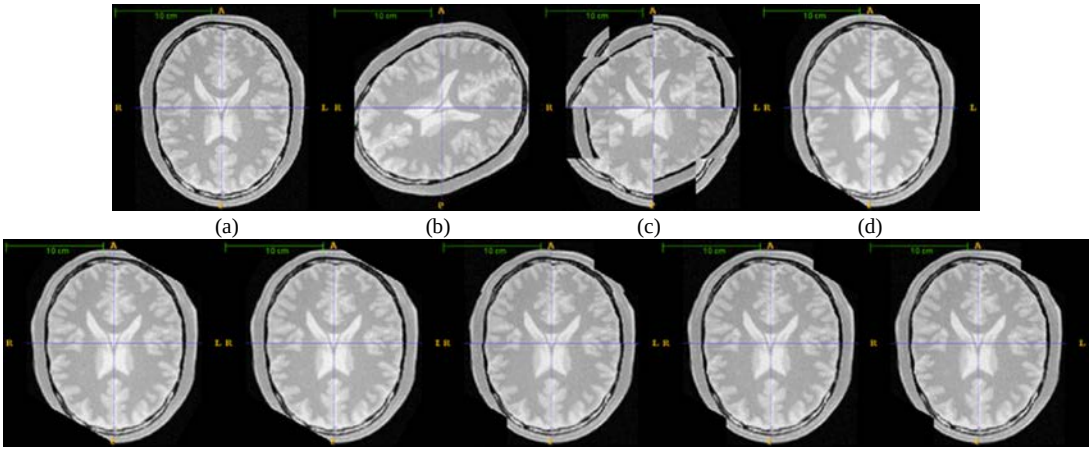

(a) (b) (c) (d)

(e) (f) (g) (h) (i)

Fig. 8. Registration results with A-NSIFT-ICP, A-NSIFT-GMM and our method for the PD-MR dataset when the rotation angle between the fixed image and the moving image is $60°$. (a), (b) and (c) separately represent the slice of the fixed image, moving image, and the chessboard differences between the moving image and the fixed image. (d), (e) and (f) are the registered images when using A-NSIFT-ICP, A-NSIFT-GMM and our method. (g), (h) and (i) are the chessboard differences of the registered image and the fixed image when using A-NSIFT-ICP, A-NSIFT-GMM and our method.

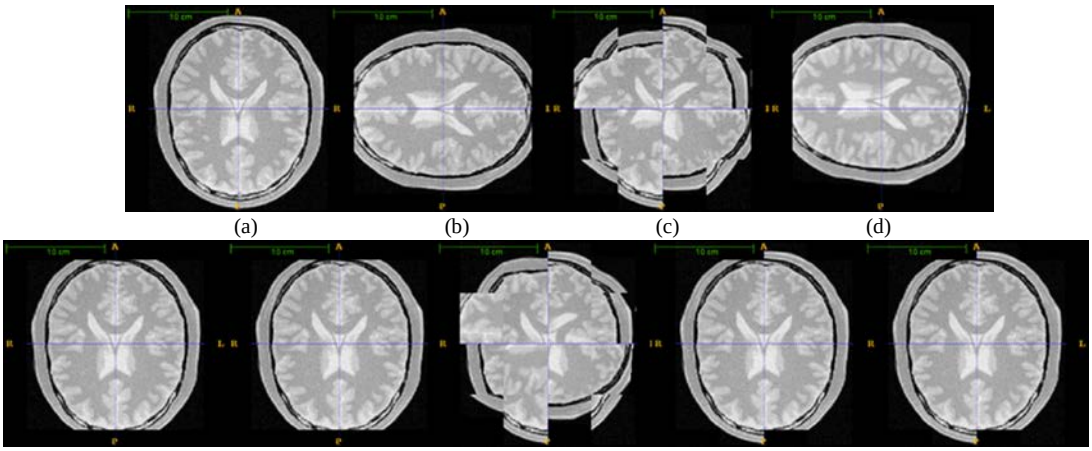

(a) (b) (c) (d)

(e) (f) (g) (h) (i)

Fig. 9. Registration results with A-NSIFT-ICP, A-NSIFT-GMM and our method for the PD-MR dataset when the rotation angle between the fixed image and the moving image is $90°$. (a), (b) and (c) separately represent the slice of the fixed image, moving image, and the chessboard differences between the moving image and the fixed image. (d), (e) and (f) are the registered images when using A-NSIFT-ICP, A-NSIFT-GMM and our method. (g), (h) and (i) are the chessboard differences of the registered image and the fixed image when using A-NSIFT-ICP, A-NSIFT-GMM and our method.

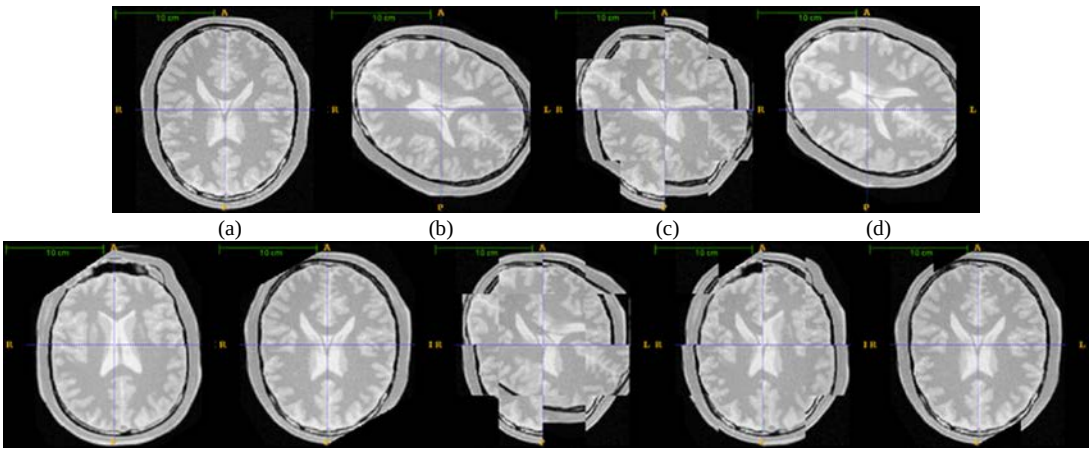

(a) (b) (c) (d)

(e) (f) (g) (h) (i)

Fig. 10. Registration results with A-NSIFT-ICP, A-NSIFT-GMM and our method for the PD-MR dataset when the rotation angle between the fixed image and the moving image is $120°$. (a), (b) and (c) separately represent the slice of the fixed image, moving image, and the chessboard differences between the moving image and the fixed image. (d), (e) and (f) are the registered images when using A-NSIFT-ICP, A-NSIFT-GMM and our method. (g), (h) and (i) are the chessboard differences of the registered image and the fixed image when using A-NSIFT-ICP, A-NSIFT-GMM and our method.

This article has been accepted for publication in a future issue of this journal, but has not been fully edited. Content may change prior to final publication. Citation information: DOI 10.1109/TBME.2015.2465855, IEEE Transactions on Biomedical Engineering

C. Clinical Cardiac DTMRI data

The performance of our proposed algorithm is also validated by a set of *ex-vivo* cardiac diffusion tensor MRI data which was acquired from 5 patients with different orientation, size and shape. Especially, their orientations vary greatly, some of which are with almost 180 degree differences. Since our algorithm focus on rigid registration, we conducted experiments on each 10 pairs and compared their orientation. When the orientation difference between the registered image and the fixed image is less than 10 degree, we consider it as a successful registration. It is found that the success rates of the A-NSIFT-ICP, the A-NSIFT-GMM, and our proposed algorithm are respectively 4/10, 3/10, and 8/10 without any denosing preprocessing. In Fig. 11 is shown a qualitative comparison with the A-NSIFT-ICP method, the A-NSIFT-GMM method and our method on two ex-vivo cardiac b0 images, whose orientation difference is almost 180 degree. We can see from Fig. 11 (c) and (d) that the A-NSIFT-ICP and the A-NSIFT-GMM do not work at all in this case. However, using our proposed method, the moving image and the fixed image are well aligned in the orientation.

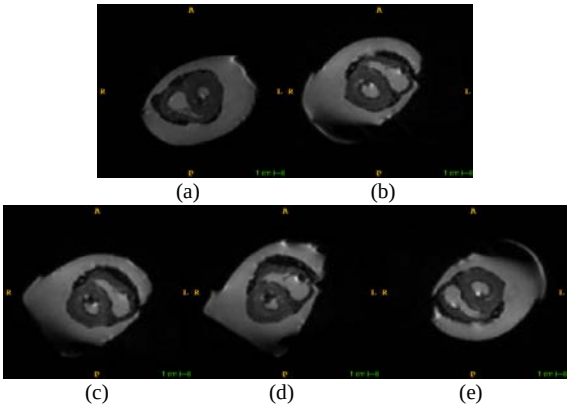

Fig. 11. Qualitative comparison on registration results with the A-NSIFT-ICP, the A-NSIFT-GMM and our proposed method on clinical cardiac DTMRI dataset. (a) and (b) separately represent the slice of the fixed image and moving image. (c), (d) and (e) are the registered images obtained from the A-NSIFT-ICP, the A-NSIFT-GMM and our method.

IV. Conclusion

In this paper, we propose a fast rotation-free feature based rigid registration algorithm based on the proposed A-NSIFT and PO-GMMREG algorithms. We first introduce a new A-NSIFT algorithm to speed up the interest point extraction. By using the A-NSIFT method, the speed is 200 times faster than the conventional NSIFT method. Then, the matching of the interest point sets is converted into the alignment of the Gaussian mixture models by representing the probability density estimation with the Gaussian mixture model, while the accuracy of the alignment on large pose differences is ameliorated by the proposed PO-GMMREG algorithm. Experimental results have validated that our proposed method is reliable for fast alignment of 3D scans even when they exhibit a poor initialization. Though the present work focuses on the improvement of the GMM method, our proposed quaternion initialization can be readily applied to most rigid point set registration algorithms to handle rigid registration problems with large pose differences.

References

[1] A. R. Khan, L. Wang, and M. F. Beg, "Multistructure large deformation diffeomorphic brain registration," *IEEE Trans. Biomed. Eng.*, vol. 60, no. 2, pp. 544–53, Feb. 2013.

[2] S. E. A. Muenzing, B. van Ginneken, M. A. Viergever, and J. P. W. Pluim, "DIRBoost-an algorithm for boosting deformable image registration: Application to lung CT intra-subject registration," *Med. Image Anal.*, vol. 18, pp. 449–459, 2014.

[3] F. Gigengack, L. Ruthotto, M. Burger, C. H. Wolters, X. Jiang, and K. P. Schäfers, "Motion Correction in Dual Gated Cardiac PET Using Mass-Preserving Image Registration," *IEEE Trans. Med. Imaging*, vol. 31, no. 3, pp. 698–712, 2012.

[4] J. Kim and J. A. Fessler, "Intensity-Based Image Registration Using Robust Correlation Coefficients," *IEEE Trans. Med. Imaging*, vol. 23, no. 11, pp. 1430–1444, 2004.

[5] A. Myronenko and X. Song, "Intensity-based image registration by minimizing residual complexity," *IEEE Trans. Med. Imaging*, vol. 29, no. 11, pp. 1882–1891, 2010.

[6] D. Shen, "Image registration by local histogram matching," *Pattern Recognit.*, vol. 40, pp. 1161–1172, 2007.

[7] Y. Ou, A. Sotiras, N. Paragios, and C. Davatzikos, "DRAMMS: Deformable registration via attribute matching and mutual-saliency weighting," *Med. Image Anal.*, vol. 15, pp. 622–639, 2011.

[8] G. K. Rohde, B. M. Dawant, and S. F. Lin, "Correction of motion artifact in cardiac optical mapping using image registration," *IEEE Trans. Biomed. Eng.*, vol. 52, no. 2, pp. 338–341, 2005.

[9] C. Studholme, C. Drapaca, B. Iordanova, and V. Cardenas, "Deformation-Based Mapping of Volume Change From Serial Brain MRI in the Presence of Local Tissue Contrast Change," *IEEE Trans. Med. Imaging*, vol. 25, no. 5, pp. 626–639, 2006.

[10] Q. Lin, Z. Liang, C. Duan, J. Ma, H. Li, C. Roque, J. Yang, G. Zhang, H. Lu, and X. He, "Motion correction for MR cystography by an image processing approach.," *IEEE Trans. Biomed. Eng.*, vol. 60, no. 9, pp. 2401–10, Sep. 2013.

[11] O. Cordón, S. Damas, and J. Santamaría, "Feature-based image registration by means of the CHC evolutionary algorithm," *Image Vis. Comput.*, vol. 24, pp. 525–533, 2006.

[12] H. Goncalves, L. Corte-Real, and J. A. Goncalves, "Automatic Image Registration Through Image Segmentation and SIFT," *IEEE Trans. Geosci. Remote Sens.*, vol. 49, no. 7, pp. 2589–2600, 2011.

[13] X. Kang, M. Armand, Y. Otake, W. Yau, P. Y. S. Cheung, S. Member, Y. Hu, and R. H. Taylor, "Robustness and Accuracy of Feature-Based Single Image 2-D – 3-D Registration Without Correspondences for Image-Guided Intervention," *IEEE Trans. Biomed. Eng.*, vol. 61, no. 1, pp. 149–161, 2014.

[14] A. Sotiras, C. Davatzikos, and N. Paragios, "Deformable Medical Image Registration: A Survey," *IEEE Trans. Med. Imaging*, vol. 32, no. 7, pp. 1153–1190, 2013.

[15] D. G. Lowe, "Distinctive Image Features from Scale-Invariant Keypoints," *Int. J. Comput. Vis.*, vol. 60, no. 2, pp. 91–110, 2004.

[16] W. Cheung and G. Hannarneh, "N-sift: N-dimensional scale invariant feature transform for matching medical images," in the 4th *IEEE International Symposium on Biomedical Imaging*, From Nano to Macro, 2007, pp. 720-723.

[17] K. Mikolajczyk and C. Schmid, "Performance evaluation of local descriptors," *IEEE Trans. Pattern Anal. Mach. Intell.*, vol. 27, no. 10, pp. 1615–1630, 2005.

[18] H. Bay, A. Ess, T. Tuytelaars, and L. Van Gool, "Speeded-Up Robust Features (SURF)," *Comput. Vis. Image Underst.*, vol. 110, pp. 346–359, 2008.

[19] E. Tola, V. Lepetit, and P. Fua, "DAISY: An efficient dense descriptor applied to wide-baseline stereo," *IEEE Trans. Pattern Anal. Mach. Intell.*, vol. 32, no. 5, pp. 815–830, 2010.

[20] M. Calonder, V. Lepetit, M. Ozuysal, T. Trzcinski, C. Strecha, and P. Fua, "BRIEF: Computing a Local Binary Descriptor very Fast," *IEEE Trans. Pattern Anal. Mach. Intell.*, vol. 34, no. 7, pp. 1281–1298, 2012.

[21] P. J. Besi and N. D. Mckay, "A Method for Registration of 3-D Shapes," in *Proc. SPIE*, Sensor Fusion IV: Control Paradigms and Data Structures, 586 vol. 1611, pp. 586–606, 1992.

[22] L. Zhang, S.-I. Choi, and S.-Y. Park, "Robust ICP Registration Using Biunique Correspondence," *3D Imaging, Modeling, Processing, Visualization and Transmission (3DIMPVT), 2011 International Conference on*, Hangzhou, Beijing, 2011, pp. 80–85.

[23] J. Chen, B. Belaton, and Z. Pan, "A Robust Subset-ICP Method for Point Set Registration," *Advances in Visual Informatics*. Springer International Publishing, 2013, pp. 59-69.

[24] C. V Stewart, C.-L. Tsai, and B. Roysam, "The dual-bootstrap iterative closest point algorithm with application to retinal image registration," *IEEE Trans. Med. Imaging*, vol. 22, no. 11, pp. 1379–94, 2003.

[25] Y. Tsin and T. Kanade, "A correlation-based approach to robust point set registration," in *Computer Vision-ECCV*, 2004, pp. 558-569.

[26] B. Jian and B. C. Vemuri, "A Robust Algorithm for Point Set Registration Using Mixture of Gaussians," in *Tenth IEEE International Conference on Computer Vision*, 2005, vol. 2, pp. 1246–1251.

[27] B. Jian and B. C. Vemuri, "Robust Point Set Registration Using Gaussian Mixture Models," *IEEE Trans. Pattern Anal. Mach. Intell.*, vol. 33, no. 8, pp. 1633–1645, 2011.

[28] J. M. Saragih, S. Lucey, and J. F. Cohn, "Deformable Model Fitting by Regularized Landmark Mean-Shift," *Int. J. Comput. Vis.*, vol. 91, no. 2, pp. 200–215, 2011.

[29] O. Zvitia, A. Mayer, R. Shadmi, S. Miron, and H. K. Greenspan, "Co-registration of white matter tractographies by adaptive-mean-shift and Gaussian mixture modeling," *IEEE Trans. Med. Imaging*, vol. 29, no. 1, pp. 132–145, 2010.

[30] H. Chui and A. Rangarajan, "A feature registration framework using mixture models," *Proceedings. IEEE Workshop on Mathematical Methods in Biomedical Image Analysis*, 2000, pp. 190-197.

[31] K. Kanatani, "Statistical Optimization for Geometric Fitting: Theoretical Accuracy Bound and High Order Error Analysis," *Int. J. Comput. Vis.*, vol. 80, pp. 167–188, 2008.

[32] Y. Kanazawa and K. Kanatani, "Do we really have to consider covariance matrices for image features?" in *Proc. Eighth IEEE Int. Conf. Comput. Vision. ICCV* , 2001, vol. 2, pp. 301–306.

[33] http://graphics.stanford.edu/data/3Dscanrep/

[34] J. M. Peyrat, M. Sermesant, X. Pennec, H. Delingette, C. Xu, E. R. McVeigh, and N. Ayache, "A computational framework for the statistical analysis of cardiac diffusion tensors: Application to a small database of canine hearts," *IEEE Trans. Med. Imaging*, vol. 26, no. 11, pp. 1500–1514, 2007.

[35] A. W. Fitzgibbon, "Robust registration of 2D and 3D point sets," *Image Vis. Comput.*, vol. 21, pp. 1145–1153, 2003.

[36] A. Myronenko and X. Song, "Point set registration: coherent point drift," *IEEE Trans. Pattern Anal. Mach. Intell.*, vol. 32, no. 12, pp. 2262–2275, 2010.